Contrast-Independent Liver-Fat Quantification from Spectral CT Exams

Paulo R.S. Mendonça[1], Peter Lamb[1], Andras Kriston[2], Kosuke Sasaki[3], Masayuki Kudo[3], and Dushyant V. Sahani[4]

[1] GE Global Research, One Research Circle, Niskayuna, NY 12309, USA
[2] GE Healthcare, Szikra u.2, Szeged, 6725, Hungary
[3] GE Healthcare Japan, 4-7-127, Asahigaoka, Hino-shi, Tokyo, Japan
[4] Massachusetts General Hospital, 55 Fruit St., Boston, MA 02114, USA
{mendonca,peter.lamb,a.kriston,kosuke.sasaki, masayuki.kudo}@ge.com, dsahani@partners.org

Abstract. The diagnosis and treatment of fatty liver disease requires accurate quantification of the amount of fat in the liver. Image-based methods for quantification of liver fat are of increasing interest due to the high sampling error and invasiveness associated with liver biopsy, which despite these difficulties remains the gold standard. Current computed tomography (CT) methods for liver-fat quantification are only semi-quantitative and infer the concentration of liver fat heuristically. Furthermore, these techniques are only applicable to images acquired without the use of contrast agent, even though contrast-enhanced CT imaging is more prevalent in clinical practice. In this paper, we introduce a method that allows for direct quantification of liver fat for both contrast-free and contrast-enhanced CT images. Phantom and patient data are used for validation, and we conclude that our algorithm allows for highly accurate and repeatable quantification of liver fat for spectral CT.

1 Introduction

Accurate quantification of liver fat is of utmost importance for the diagnosis, characterization, and treatment of fatty liver disease [2]. This need is highlighted since early diagnosis can prevent the onset of more serious liver diseases and associated health risks [12], and even reverse forms of fatty liver disease [1]. Furthermore, concentration of liver fat is an important clinical consideration in liver resection [6].

Although liver biopsy is still accepted as the gold standard for liver-fat quantification, results are often disputed due to sampling error. Non-invasive imaging with magnetic resonance (MR), ultrasound (US), and computed tomography (CT), therefore, is of increasing interest [11]. Of these three modalities, MR is most often cited as the superior choice for liver-fat quantification [6,9]. However, alternatives to MR are desired since it is a costly and time-consuming exam [9]. The use of US in liver-fat quantification is disputed due to prevalent concerns about inexact quantification methods and inter-observer and inter-equipment reproducibility of results [2,13].

Three techniques currently exist for the quantification of liver fat with CT, and all rely on the assumption of an approximate inverse relationship between liver-fat content and liver attenuation [13]. The first method is the direct measurement of liver attenuation

K. Mori et al. (Eds.): MICCAI 2013, Part I, LNCS 8149, pp. 324–331, 2013.

in Hounsfield units (HU). The second and third techniques compute the average HU value of the liver and of the spleen, and then compute differences (liver minus spleen) or ratios (typically, spleen to liver). The use of the spleen, however, has not necessarily proven to be a better metric than direct measurement of liver attenuation [6].

The key limitation of these three methods is that they are impractical for contrast-enhanced CT acquisitions [6], where the presence of contrast agent greatly skews HU values. Spectral CT has offered a solution to the contrast-enhanced limitation via material decomposition, a technique that allows for the virtual removal of contrast from contrast-enhanced images, or *virtual un-enhancement* (VUE) [5,7]. However, liver-fat quantification via VUE ultimately relies on heuristic rules mapping HU values and fat content, and thus remains semi-quantitative in nature [12].

We propose a method for direct and accurate quantification of liver fat using spectral CT. Results on phantom data were compared to the MR IDEAL IQ technique [10], an MR-based method for liver-fat quantification. Results verify repeatability for both contrast-free and contrast-enhanced scans, thereby increasing the clinical usefulness of CT for the treatment of patients with fatty liver disease.

2 Material Decomposition via Spectral CT

Spectral CT explores the dependence of linear attenuation coefficient on x-ray energy to generate CT images decomposed into a *material basis*, typically including a water and an iodine component. Key to many material decomposition methods is the assumption that the mix of materials in the human body behaves as an *ideal solution* which, among many equivalent definitions, can be described as a mixture for which a volume-preservation law applies. Under such a model, it can be shown that the linear attenuation coefficient $\mu_{\mathrm{L}}(E)$ at energy E of a mixture of N materials, each with linear attenuation coefficient $\mu_{\mathrm{L},i}(E)$, is given by $\mu_{\mathrm{L}}(E) = \sum_{i=1}^{N} \alpha_i \mu_{\mathrm{L},i}(E)$, where α_i is the volume fraction of the i-th material in the mix, such that $\sum_{i=1}^{N} \alpha_i = 1$ and $\alpha_i \geq 0$ [8].

Spectral CT data consists of a pair of water and iodine density images, denoted $\rho_{\mathrm{H_2O}}$ and ρ_{I}. This image pair is converted into images in units of linear attenuation at two pre-specified photon energies E_i, $i = 1,2$, according to the expression $\mu_{\mathrm{L}}(E_i) = \rho_{\mathrm{H_2O}}\mu_{\mathrm{M,H_2O}}(E_i) + \rho_{\mathrm{I}}\mu_{\mathrm{M,I}}(E_i)$, where $\mu_{\mathrm{M},*}(E_i)$ is the (density-independent) *mass attenuation coefficient* of material "$*$" at energy E_i, readily obtained from standardized tables [4]. For a fixed pair of photon energies E_j, $j = 1,2$, we define $\boldsymbol{\mu}_{\mathrm{L},*} = (\mu_{\mathrm{L},*}(E_1), \mu_{\mathrm{L},*}(E_2))$ for an arbitrary material "$*$". For a mix with materials $i = 1,2,3$, we have

$$\begin{bmatrix} \boldsymbol{\mu}_{\mathrm{L},1} & \boldsymbol{\mu}_{\mathrm{L},2} & \boldsymbol{\mu}_{\mathrm{L},3} \\ 1 & 1 & 1 \end{bmatrix} \begin{bmatrix} \alpha_1 \\ \alpha_2 \\ \alpha_3 \end{bmatrix} = \begin{bmatrix} \boldsymbol{\mu}_{\mathrm{L}} \\ 1 \end{bmatrix} \text{ subject to } 0 \leq \alpha_i \leq 1,\ i = 1,2,3. \tag{1}$$

The complex compositional makeup of organs and tissues in the human body imposes great difficulties for material decomposition methods that can cope with only two or three materials in the material basis. This is particularly relevant for CT-based liver-fat quantification, in which fat, blood, liver tissue, and contrast agent are present. To address this problem, we propose an algorithm consisting of a sequence of two independent material decompositions of spectral CT data.

3 Algorithms and Methods

The input for the proposed liver-fat quantification algorithm can be either contrast-free or contrast-enhanced spectral CT data. In the contrast-enhanced case, *virtual un-enhancement* [5,7] is applied to produce images from which the effect of contrast enhancement has been digitally removed. In the contrast-free case, the VUE step is skipped and fat quantification can be directly performed.

3.1 Virtual Un-Enhancement of the Liver

To achieve consistency between contrast-free and contrast-enhanced results, we apply an algorithm for *virtual un-enhancement* (VUE) [5,7] to contrast-enhanced data. VUE produces images from which the effect of contrast enhancement has been removed. This is achieved by applying (1) using fat, blood, and contrast agent as the material triplet. General VUE methods make use of a non-negativity constraint over the parameters α_i in (1) as an indicator to select, among a large number of material triplets, which one is most adequate to represent the input data at a given voxel. For an appropriate selection, the condition $0 \leq \alpha_i \leq 1$, $i = 1,2,3$ should be immediately satisfied. Since the focus of our application is on liver-fat quantification, we are not concerned about representing materials such as bone or calcifications, which are typical confounding factors for general VUE methods. Moreover, we may also disregard the constraint $\alpha_i \geq 0$ introduced in [8]. In the specific context of liver-fat quantification, and assuming a fat ($i = 1$), blood ($i = 2$), and contrast agent ($i = 3$) material triplet, the violation of this constraint may in fact be expected. Healthy liver tissue, for example, has a higher attenuation than that of blood, in which case the equations $\sum_{i=1}^{3} \alpha_i \mu_{\mathrm{L},i}(E_j) = \mu_{\mathrm{L}}(E_j)$ and $\sum_{i=1}^{3} \alpha_i = 1$, for photon energies E_1 and E_2, can only be satisfied if α_1 is negative. Furthermore, the presence of noise may result in the above equations yielding a slightly negative value for α_3 in the case of contrast-free exams.

Once the decomposition in (1) is completed and the coefficients α_i, $i = 1,2,3$ are obtained, we proceed as in [7] and *replace* the contrast agent component of a voxel by its equivalent volume in blood, thereby producing a final VUE image with linear attenuation coefficients $\mu'_{\mathrm{L}}(E_j)$ given by $\mu'_{\mathrm{L}}(E_j) = \alpha_1 \mu_{\mathrm{L},1}(E_j) + (\alpha_2 + \alpha_3)\mu_{\mathrm{L},2}(E_j)$, for photon energies E_j, $j = 1,2$. Graphically, this corresponds to the projection operation indicated by the arrow mapping "Input data" to "VUE" depicted in Fig. 1.

3.2 Fat Quantification of the Liver

For contrast-free spectral CT data, or for contrast-enhanced spectral CT data after the application of VUE, fat quantification is performed through dual-material decomposition using fat and healthy liver tissue as the material pair. The energy-dependent linear attenuation coefficient of healthy liver tissue is not directly available from standardized tables, and we therefore obtained it experimentally. Note that this is an off-line process, executed only once prior to algorithm implementation, and the resulting attenuation coefficient is valid for any input clinical data. To obtain the coefficient of healthy liver tissue, we first observed that the contrast-free (or VUE) attenuation of healthy liver tissue is accurately represented as a point along the line connecting the linear attenuations

of fat and blood, as shown in Fig. 2. We then manually selected several regions of interest (ROIs) of healthy livers from images in our patient dataset. The linear attenuation coefficients at energies E_j, $j = 1,2$ for the data of the selected ROIs was extracted, resulting in a set $\{\boldsymbol{\mu}^k_{\mathrm{L,liver}}, k = 1,\ldots,K\}$, where K is the total number of voxels within the ROIs. Finally, we solve the simple convex optimization problem

$$\boldsymbol{\mu}_{\mathrm{L,liver}} = \arg\min_{\boldsymbol{\mu}_{\mathrm{L}}} \sum_{k=1}^{K} \|\boldsymbol{\mu}_{\mathrm{L}} - \boldsymbol{\mu}^k_{\mathrm{L,liver}}\|^2 \tag{2a}$$

$$\text{subj.} \begin{vmatrix} \boldsymbol{\mu}_{\mathrm{L,fat}} & \boldsymbol{\mu}_{\mathrm{L,blood}} & \boldsymbol{\mu}_{\mathrm{L}} \\ 1 & 1 & 1 \end{vmatrix} = 0 \tag{2b}$$

yielding $\boldsymbol{\mu}_{\mathrm{L,liver}}$ (which corresponds to the large green point shown in Fig. 2). The basic cost function in (2a) favors estimates of $\boldsymbol{\mu}_{\mathrm{L,liver}}$ that are good approximations for the training data, and the constraint on the determinant of the 3×3 matrix in (2b) enforces that the points corresponding to the linear attenuations of fat, blood, and liver at energies E_j, $j = 1,2$ are indeed aligned.

By imposing the constraint expressed in (2b), we can perform fat quantification on contrast-free (or VUE) data through dual-material decomposition, and the liver-fat quantification problem is now formulated as

$$\begin{bmatrix} \boldsymbol{\mu}_{\mathrm{L},1} & \boldsymbol{\mu}_{\mathrm{L,liver}} \\ 1 & 1 \end{bmatrix} \begin{bmatrix} \alpha_1 \\ \alpha_{\mathrm{liver}} \end{bmatrix} = \begin{bmatrix} \boldsymbol{\mu}_{\mathrm{L}} \\ 1 \end{bmatrix} \tag{3}$$

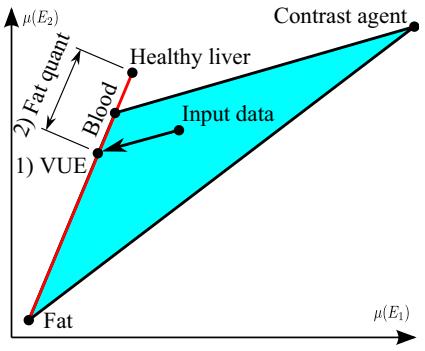

Fig. 1. Steps of liver-fat quantification algorithm. For contrast-enhanced spectral CT data, we first apply VUE to digitally remove the effect of contrast enhancement. After VUE, or for contrast-free spectral CT data, fat quantification is performed through dual-material decomposition using fat and healthy liver as the material pair.

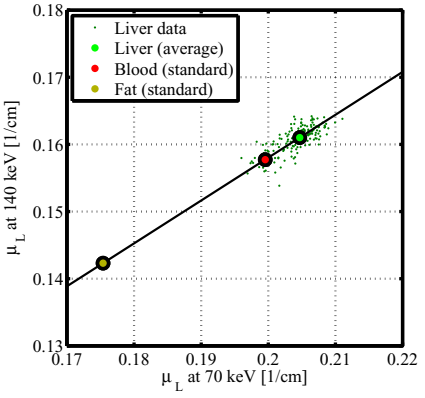

Fig. 2. Linear attenuation coefficient of healthy liver tissue. Whereas the linear attenuation coefficients of fat (large gold point) and blood (large red point) can be obtained from standardized tables, the linear attenuation coefficient of healthy liver tissue (large green point) had to be derived experimentally.

Table 1. Fat quantification results on phantom data. The table shows mean (μ) and standard deviation (σ) of the results of fat quantification for phantom data. Results of the proposed CT algorithm are quantitatively accurate, performing comparably to the MR IDEAL IQ technique.

Ground truth	0%	10%	20%	30%	50%	100%
CT % fat ($\mu \pm \sigma$)	1.1 ± 1.5	8.8 ± 2.6	16.8 ± 2.8	27.0 ± 2.6	46.5 ± 3.0	97.2 ± 1.9
MR % fat ($\mu \pm \sigma$)	1.8 ± 1.7	13.1 ± 1.7	23.9 ± 1.6	34.2 ± 1.1	53.0 ± 1.2	99.6 ± 0.9

subject to $0 \leq \alpha_i \leq 1$, $i = 1,$ liver. Note that now we do impose the inequality constraints over the volume fractions α, so as to avoid (due to noise) a volume fraction that is either negative or greater than 100%. For VUE data, (3) could be exactly satisfied if it were not for the inequality constraints. For contrast-free data (which does not undergo VUE), the inequality constraints can be violated (and may never be satisfied) since (3) is a linear system of three equations in two variables. Therefore, for both VUE and contrast-free data the final fat quantification result $\boldsymbol{\alpha} = (\alpha_{\text{fat}}, \alpha_{\text{liver}})$ is obtained through the solution of a convex constrained least-squares problem, given by

$$\begin{aligned} \boldsymbol{\alpha}(\boldsymbol{x}) = \arg\min_{\boldsymbol{\alpha}^*} \left\| \begin{bmatrix} \boldsymbol{\mu}_{\text{L,fat}} & \boldsymbol{\mu}_{\text{L,liver}} \\ 1 & 1 \end{bmatrix} \boldsymbol{\alpha}^* - \begin{bmatrix} \boldsymbol{\mu}_{\text{L}}(\boldsymbol{x}) \\ 1 \end{bmatrix} \right\|^2 \\ \text{subj.} \sum_{i=1}^{2} \alpha_i^* = 1, \alpha_i^* \geq 0, i = 1,2. \end{aligned} \tag{4}$$

Typically, material concentrations are reported as mass fractions, which we denote by β. An elementary calculation then yields $\beta_{\text{fat}} = \alpha_{\text{fat}}\rho_{\text{fat}}/(\alpha_{\text{fat}}\rho_{\text{fat}} + \alpha_{\text{liver}}\rho_{\text{liver}})$. The dependency of $\boldsymbol{\alpha}$ on $\boldsymbol{x}$ has been introduced in (4) to highlight that the input data $\boldsymbol{\mu}_{\text{L}}$ (or $\boldsymbol{\mu}_{\text{L}}(\boldsymbol{x})$) is the pair of linear attenuation coefficients at energies E_1 and E_2 *at the voxel* $\boldsymbol{x}$, and that the complete algorithm is executed for every voxel within the liver, naturally lending itself towards a parallel implementation. Furthermore, only two inputs in $\boldsymbol{\mu}_{\text{L}}(\boldsymbol{x})$ are required for each voxel, allowing further speed improvements through the use of lookup tables. Our implementation can process over 1.5×10^7 voxels (the size of a typical abdominal CT exam) per second on a 3.2 GHz quad-core Intel Xenon system.

4 Experiments and Results with Phantoms

Clinical ground truth for liver-fat content is difficult; even biopsy may be misleading, due to sampling errors. Therefore we used a physical phantom with carefully measured fat content as our ground truth for evaluating accuracy. Pig liver (in food) and titrated fat (lard) were mixed homogeneously to simulate fatty liver with concentrations of 0%, 10%, 20%, 30%, 50%, and 100% fat (by mass) and scanned using a GE Discovery CT750 HD scanner. For comparison, two MR scans were also performed using a GE Discovery MR750W and the commercially available IDEAL IQ technique [10], which provides a quantitative assessment of triglyceride fat content in the liver.

Fat quantification results for the phantom data using our algorithm are shown in Table 1. MR results using the IDEAL IQ technique are also presented for comparison.

While the MR results have a slightly smaller variance, our CT results have a smaller bias. Note that MR-based fat quantification methods, such as IDEAL IQ, face a number of confounding factors such as T_1 bias, T_2^* decay, multiple fat peaks, noise bias, and eddy currents [3]. Furthermore, these techniques actually measure proton density fat fraction, which is correlated, but not equivalent, to true mass fat fraction. With this in mind, our results indicate that the proposed algorithm can match the performance of MR-based fat quantification methods, thereby increasing the clinical utility of CT.

5 Experiments and Results with Clinical Data

Study protocol was reviewed and approved by an institutional review board in Kinki University Hospital (Osaka-sayama City, Osaka, Japan) and informed consent was obtained from all participants. Spectral CT imaging was performed using a GE Discovery CT750 HD scanner on fifty patients with various stages of fatty liver disease. Multi-phase scans consisting of contrast-free and contrast-enhanced (at the arterial, portal venous, and delayed) phases were acquired. Note that all patients underwent contrast-free scanning, but not all contrast-enhanced phases of scanning (13 patients underwent arterial phase scanning, 50 patients underwent portal venous phase scanning, and 40 patients underwent delayed phase scanning). The proposed algorithm was run on all

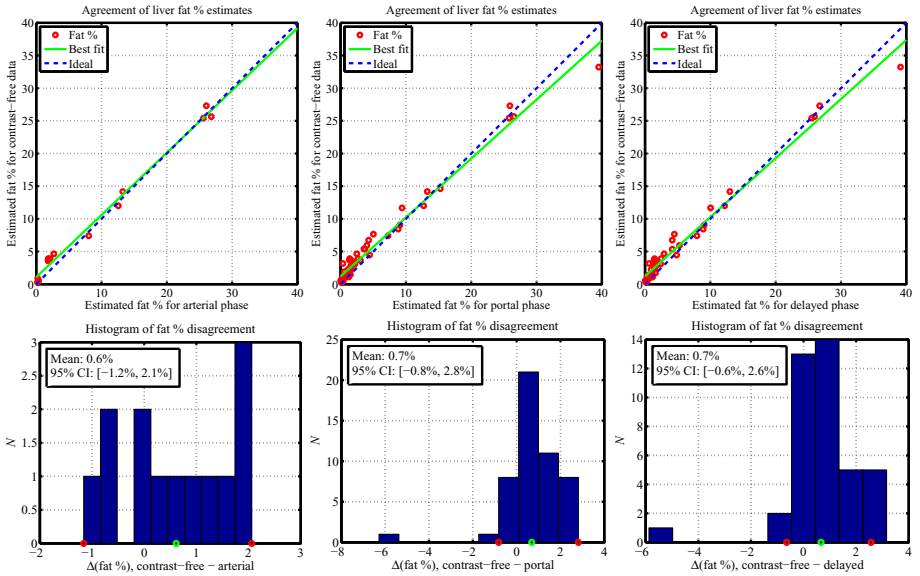

Fig. 3. Repeatability of clinical liver-fat quantification results. Top row: Scatterplots of liver-fat quantification results. Each red circle is the average liver-fat % reported by our algorithm for the contrast-free phase plotted against a particular contrast-enhanced phase. The dotted blue line is the region of perfect agreement. The solid green line is a fit to our results. Bottom row: Histograms of differences between the contrast-free and contrast-enhanced fat quantification results, with mean (green circle) and 95% confidence intervals (red circles) reported.

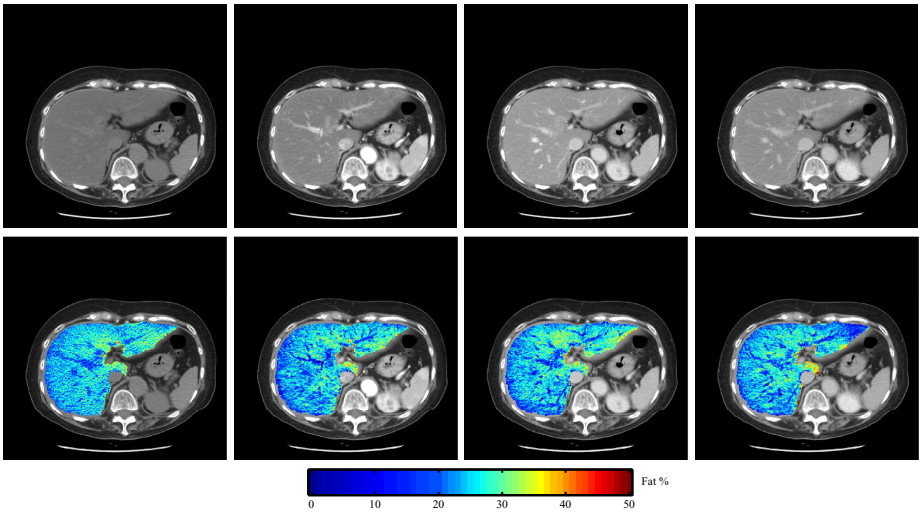

Fig. 4. Overlay of fat quantification results. Top row: From left to right, registered CT images of non-contrast, arterial, portal venous, and delayed phases of a liver exam. Bottom row: Overlay of fat % maps obtained from the proposed algorithm, showing consistent fat quantification results across all phases of imaging. Images are roughly aligned, but not fully registered.

multi-phase images, and liver-fat quantification results were aggregated on a 3D-basis for the voxels of the liver. Patient data is courtesy of Prof. Takamichi Murakami (Kinki University: Osaka-sayama City, Osaka, Japan).

Naturally, the concentration of hepatic fat of a given patient does not change with the injection of contrast agent. As shown in Fig. 3, all but one of the estimated fat concentrations for the contrast-enhanced scans are within ± 3 %, in absolute terms, of the estimated fat concentration for the contrast-free scans. (The single exception comes from an exam severely corrupted by metal artifacts.) This demonstrates a key benefit of the present work: The consistent ability to estimate fat concentration regardless of the presence of contrast agent or the phase of imaging. As shown in Fig. 4, our algorithm produces consistent results across all phases of imaging. This naturally allows clinicians to incorporate our algorithm into any stage of their liver imaging workflow. Furthermore, fat % maps such as the ones displayed in Fig. 4 allow for easy visualization of the spatial distribution of fat content in the liver, which can greatly aid in procedures such as biopsy and surgery planning.

6 Conclusion

In this paper, we have presented a novel method for the accurate and repeatable quantification of liver fat using spectral CT. The innovation of this work lies in a sequential approach for material decomposition, which allows for liver-fat quantification for both contrast-free and contrast-enhanced images. We validate our algorithm with phantom data, which demonstrates absolute quantitative accuracy, and clinical data, which

demonstrates the repeatability of the algorithm across multi-phase imaging. Results indicate that our algorithm has the potential to improve the utility of CT — and perhaps even obviate the need for biopsy — for the diagnosis, characterization, and treatment of fatty liver disease. Future work will extend the capabilities of the algorithm to allow for the detection and characterization of iron deposition, thus providing a more comprehensive tool for the analysis of patients with fatty liver disease.

References

1. Asano, K., Bayram, E., Yu, H., Reeder, S.B.: Quantitative fat imaging for evaluating diffuse liver diseases. In: SignaPULSE, pp. 75–78. GE Healthcare (2011)
2. Duman, D., Celikel, C., Tüney, D., Imeryüz, N., Avsar, E., Tözün, N.: Computed tomography in nonalcoholic fatty liver disease. Digestive Diseases and Sciences 51(2), 346–351 (2006)
3. Hu, H.H., Börnert, P., Hernando, D., Kellman, P., Ma, J., Reeder, S., Sirlin, C.: ISMRM workshop on fat-water separation: Insights, applications and progress in MRI. Magnetic Resonance in Medicine 68(2), 378–388 (2012)
4. Hubbell, J.H., Seltzer, S.M.: Tables of X-ray mass attenuation ceofficients and mass energy-absorption coefficients. Technical Report NISTIR 5632, National Institute of Standards and Technology, Gaithersburg, MD, USA (May 1995)
5. Johnson, T.R.C., Krauß, B., Sedlmair, M., Grasruck, M., Bruder, H., Morhard, D., Fink, C., Weckbach, S., Lenhard, M., Schmidt, B., Flohr, T., Reiser, M.F., Becker, C.R.: Material differentiation by dual energy CT: Initial experience. European Radiology 17(6), 1510–1517 (2007)
6. Kodama, Y., Ng, C.S., Wu, T.T., Ayers, G.D., Curley, S.A., Abdalla, E.K., Vauthey, J.N., Charnsangavej, C.: Comparison of CT methods for determining the fat content of the liver. Am. J. Roentgenol. 188(5), 1307–1312 (2007)
7. Maddah, M., Mendonça, P.R.S., Bhotika, R.: Physically meaningful virtual unenhanced image reconstruction from dual-energy CT. In: IEEE Int. Symposium on Biomedical Imaging: From Nano to Macro, Rotterdam, The Netherlands (April 2010)
8. Mendonça, P.R.S., Bhotika, R., Thomsen, B.W., Licato, P.E., Joshi, M.C.: Multi-material decomposition of spectral CT images. In: SPIE Medical Imaging, San Diego, CA, USA, vol. 7622, pp. 76221W–76221W-9 (February 2010)
9. Patel, K.D., Abeysekera, K.W.M., Marlais, M., McPhail, M.J.W., Thomas, H.C., Fitzpatrick, J.A., Lim, A.K.P., Taylor-Robinson, S.D., Thomas, E.L.: Recent advances in imaging hepatic fibrosis and steatosis. Eur. J. Gastr. Hepat. 5(1), 91–104 (2011)
10. Reeder, S.B., Robson, P.M., Yu, H., Shimakawa, A., Hines, C.D.G., McKenzie, C.A., Brittain, J.H.: Quantification of hepatic steatosis with MRI: The effects of accurate fat spectral modeling. J. Magn. Reson. Imaging. 29(6), 1332–1339 (2009)
11. Sanai, F.M., Keeffe, E.B.: Liver biopsy for histological assessment: The case against. Saudi J. Gastroenterol. 16(2), 124–132 (2010)
12. Sanyal, A.J.: American Gastroenterological Association. AGA technical review on nonalcoholic fatty liver disease. Gastroenterology 123(5), 1705–1725 (2002)
13. Schwenzer, N.F., Springer, F., Schraml, C., Stefan, N., Machann, J., Schick, F.: Non-invasive assessment and quantification of liver steatosis by ultrasound, computed tomography and magnetic resonance. J. Hepatology 51(3), 433–445 (2009)